Polymer Chemistry

3D Printing of Self-Healing, High Strength, and Reprocessable Thermoset

Journal:	*Polymer Chemistry*
Manuscript ID	PY-ART-06-2020-000819.R1
Article Type:	Paper
Date Submitted by the Author:	23-Aug-2020
Complete List of Authors:	Yuan, Tianyu; University of Michigan, Macromolecular Science and Engineering Zhang, Lisha; University of Michigan, Ann Arbor, Macromolecular Science & Engineering Li, Tony; University of Michigan, Aerospace Engineering Tu, Ruowen; University of Michigan, Aerospace Engineering Sodano, Henry; University of Michigan, Aerospace Engineering; University of Michigan,

3D Printing of Self-Healing, High Strength, and Reprocessable Thermoset

Received 00th January 20xx,
Accepted 00th January 20xx

DOI: 10.1039/x0xx00000x

Tianyu Yuan, [a] Lisha Zhang, [a] Tony Li, [b] Ruowen Tu, [b] Henry A. Sodano*[a,b,c]

Direct ink writing (DIW) is a 3D printing technique that can fabricate user-defined thermoset objects via ink extrusion and solidification. Here we demonstrate the development of a novel ink for DIW that can be used for the fabrication of a high strength, self-healing thermoset. The ink exhibits a tensile strength of 77 MPa after cure, which is comparable to that of engineering-grade epoxies. The low viscosity of the ink effectively eliminates voids between the deposited filaments, thus achieving isotropic mechanical properties of the printed thermoset. The thermally reversible Diels-Alder (DA) reaction between furan and maleimide allows the reversible formation of DA cross-links in the polymer and a high recovery (~85%) of polymer strength after the first occurrence of damage. Repeatable healing is achieved for the thermoset without a significant decrease in healing performance after three damage-healing cycles. The isotropic characteristic leads to little deterioration in the healing performance of the thermoset printed in different directions, compared with that of the molded ones. Finally, unlike most thermosetting materials, the developed thermoset is reprocessable and can be remolded. This work shows the potential for 3D printing thermosets composed of furan/maleimide monomers to produce strong, self-healing, and recyclable 3D printed materials.

Introduction

Three-dimensional printing (3DP) has been widely studied over the past two decades because it enables the fabrication of flexible and high dimensional resolution objects using a variety of materials. Metals,[1] composites,[2] thermoplastics,[3] and thermoset materials[4] have all shown great 3DP potential for applications in the field of smart devices,[5] biomedicine,[6] vehicle manufacturing,[7] etc. Among these 3DP materials, thermosets have attracted a growing interest in the field of structural materials due to their excellent mechanical performance and low density. For example, epoxy and bismaleimide resin are two common commercially available thermosets, which have a tensile strength of ~80 MPa[8,9], making them ideal for the construction of structural composites. However, the cross-linked nature of thermosets is inherently incompatible with 3D printing techniques and result in challenging processing methods. Two primary strategies have been adopted to overcome such processing issues: (1) UV curing; and (2) thermal curing, as both approaches are capable of facilitating the formation of thermosets during or after printing. The rapid curing cycle of UV-curable printing systems is usually achieved by the fast initiation of photopolymerization. Schimph *et al.*[10] reported a photo-curable hydroxyurethane methacrylate (HUMA) resin for 3D printing that exploits the rapid initiation of photo-initiator and can be cured within 1.5-2 s per layer. However, the UV curing process usually requires the use of photo-initiators and excess amounts of curing resins in the printing pool,[11] thus reducing the cost-efficiency of the printing process. Unlike UV curing, the thermal curing process typically occurs by the deposition of printed resins on a surface and curing at an elevated temperature.[12] Such an approach does not require excess resins or photo-initiators, making thermal curing a more economical option when using conventional 3D printing setup.

For the 3DP of thermally cured thermosets, fused filament fabrication (FFF) and direct ink writing (DIW) are two of the most prominent techniques. Compared to thermoset printing, FFF is more frequently studied as a thermoplastic printing technique, because the printing procedure is more compatible with thermoplastics, which inherently have better processability than thermosets. During the printing process of FFF, the solid filament is melted at the heated nozzle and deposited at the printing platform, allowing for the building of three-dimensional objects using a layer by layer deposition approach.[13] With the processes of FFF considered, thermoset printing requires meltable thermosetting filaments, which have always been challenging to develop over the years. However, Yang *et al.*[14] overcame such a problem through the incorporation of thermally reversible Diels-Alder (DA) cross-links into the printed thermoset. The solid printing material was synthesized via DA reaction between a commercially available bismaleimide (BMI-1700) and multi-furan monomers (ICN3F, 3F, and 4F), and can be melted at

[a] Department of Macromolecular Science and Engineering, University of Michigan, Ann Arbor, MI 48109, USA.
[b] Department of Aerospace Engineering, University of Michigan, Ann Arbor, MI 48109, USA.
[c] Department of Materials Science and Engineering, University of Michigan, Ann Arbor, MI 48109, USA.
Email: hsodano@umich.edu
†Electronic Supplementary Information (ESI) available: [^{1}H NMR spectra, optical microscopic images, mechanical testing data and self-healing efficiency data].

printing temperatures of 130-140 °C, due to the cleavage of DA linkages through retro DA reaction. BMI-1700 is a linear oligomer with a molecular weight of 1715 daltons and only two maleimide groups for the DA/retro DA reaction, leading to a low cross-link density in the printing material. This feature brings about smooth printing resulting from the fast melting of the material at retro DA temperature, however, it also causes problems like weak tensile properties (18-23 MPa). Although a low cross-link density is required in the FFF printing material to realize a fast and steady printing, the mechanical properties of the prints can be weakened at the same time. Therefore, given the strict requirements of rapid melting, FFF technique is restricted by the molecular structure and mechanical properties of the printed thermosets.

Unlike FFF, DIW does not require the fast melting of solid printing resins. Instead, viscous printing ink of the desired material is extruded through a nozzle and then solidified on a substrate.[15] DIW printing inks typically possess unique rheological properties, such as low viscosity and shear-thinning,[16] thus ensuring their smooth extrusion out of printing nozzles. In the case of thermosets, the printing ink is generally a combination of monomers or oligomers, and other additives including diluents or thickeners. When an external stimulus (heat, light, etc.) is applied to the ink, the polymerization of the monomers or oligomers will be initiated and facilitate the formation of thermosets. Thermal treatment is a prevalently used technique for ink curing because it enables a wide range of cross-linking reactions such as Diels Alder reaction,[14] epoxy-carboxyl reaction,[15] and trimerization of cyanate,[17] etc. Shi *et al.*[15] developed a recyclable 3DP vitrimer epoxy thermoset using a printing ink consisting of diglycidyl ether of bisphenol A (DGEBA), fatty acids Pripol 1040, and thickener nanoclay. However, the resulting thermoset was a soft polymer with a tensile strength of 5.5 MPa and a tensile strain of 90%, as fatty acids are not good candidates for constructing strong materials. Therefore, although DIW is a simple and cost-efficient 3DP technique for the fabrication of thermally curable thermoset, challenges still remain in developing printing inks that satisfy rheological requirements, while also maintaining the excellent mechanical properties of the printed thermosets. In addition to thermal treatment, UV-treatment is another common type of curing method, which usually activates the photo-initiator and facilitates the polymerization of vinyl groups. Kuang *et al.*[18] combined UV and thermal curing in the DIW processes to construct a self-healing and shape memory elastomer. The ink was a mixture of vinyl monomers, photo-initiator Irgacure 819, polycaprolactone (PCL), and silica as the rheology modifier. For each printed layer, the ink was deposited on the printing platform and then cured by UV light to polymerize the vinyl monomers. After the printing process, the prints were post-cured by thermal treatment to induce the crystallization of PCL and form a semi-interpenetrating polymer network. Assisted by UV treatment, the prints exhibited a high printing resolution due to the fast solidification of the resin and complex hierarchical structures can be therefore achieved. Yet the built-in-house printing setup involves a heating syringe, a pneumatic system, a UV light-emitting diodes (LEDs), as well as a moving platform, which requires a lot of modifications compared to commercial printing systems. In general, efficient and straightforward printing procedures and material processing are desired for DIW system design and have attracted attention in recent years. Berry *et al.*[19] utilized a thiol-Michael reaction catalyzed by basic buffer solution to cure the prints. Using a conventional DIW setup, they printed hydrogels containing Pluronic F127 micelles with vinyl end groups and thiol crosslinkers, followed by cross-linking of the hydrogel in basic phosphate-buffered saline (PBS) solution. The printing process and the post-cure of the prints are easy to implement, only involving simple printing setup and ambient curing conditions. Nevertheless, they also mentioned the hydrolysis of the ester groups in thioether after cure, leading to a decreased modulus overtime. Besides the simplicity of printing and post-print processing, the chemical stability of the DIW prints still needs to be evaluated when designing the ink compositions in order to achieve the optimal mechanical performance of the material.

Besides investigating the mechanical properties of the prints, embedding functionality such as high thermo-oxidative stability,[17] conductivity,[20] and self-healing[21] in the printed material has been another interesting topic in the development of DIW ink for thermoset fabrication. Among all these unique properties, self-healing has attracted growing interest in material design for its potential to improve the life span of the thermoset through the in-situ repair of cracks within the polymer without the addition of any additional reactants or catalysts. Two major strategies have been prevalently employed to design self-healing thermosets: (1) extrinsic healing and (2) intrinsic healing. Extrinsic healing is enabled by the release of healing agents packaged in capsules[22] or vessels,[23] and the polymerization of the healing agents upon the damage site.[24] Since the healing does not occur inherently within the thermoset, the polymer composition and molecular design of the matrix can be rather flexible. However, after the rupture of the encapsulating shell, the healing agents are depleted, therefore limiting such an approach to a singular healing event. On the other hand, intrinsic healing is facilitated by reversible molecular interactions including hydrogen bonding, ionic interactions, and reversible covalent bonding, all of which can potentially contribute to the polymer network formation, thus enabling multiple-time and repeatable repair of the materials.[25] In contrast with hydrogen bonding and ionic interaction, reversible covalent bonds have higher bonding energies and usually lead to higher mechanical properties of the materials.

One of the most applicable reversible cross-linking reactions for self-healing thermoset synthesis is the reversible DA cycloaddition between furans and maleimides. Furan/maleimide pairs undergo DA condensation at 60-80 °C and the retro DA cleavage at a higher temperature (110-140 °C).[26] This thermally reversible feature enables the thermal healing of the thermoset with the furan/maleimide pairs. The healing procedure involves the uncoupling of the furan/maleimide pairs at the cleaving temperature, molecular movements in the polymer network, and furan/maleimide coupling at the condensation temperature. Chen *et al.*[27] first incorporated furan and maleimide in monomer structures to produce a thermally healable thermoset that demonstrated a healing efficiency of 57%. The healing performance of DA incorporated polymers was further improved by Heo *et al.*[28] In this polymeric system, diols carrying furan/maleimide groups were synthesized and reacted with isocyanates to yield a self-healing polyurethane with a high healing efficiency of up to 84 %. In contrast with other materials containing polymers with furan/maleimide side groups,[29,30] the two polymeric systems discussed above were formed

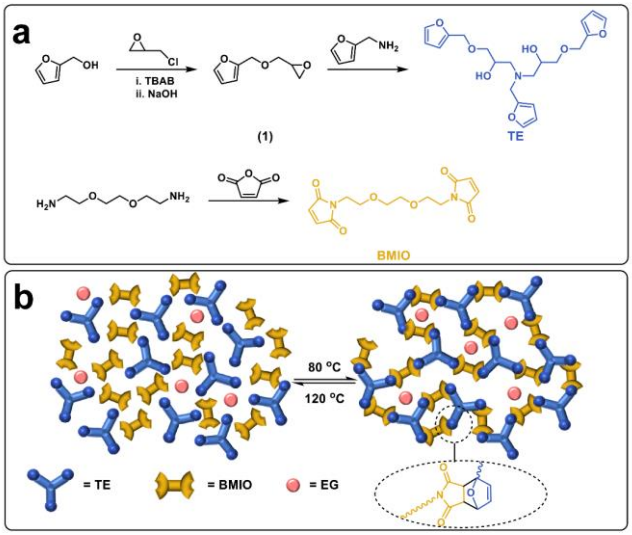

Fig. 1 (a) Synthesis of multi-furan/maleimide monomers trifuran epoxy (TE) and 1,2-bis(2-maleimidoethoxy)ethane (BMIO). (b) Thermally reversible formation of the TE-BMIO-EG thermoset.

through small molecules bearing multiple furan/maleimide groups, thus ensuring better molecular mobility at healing temperature and resulting in higher polymer healing efficiency.

Combining 3DP and self-healing functionality can potentially fabricate thermosets of complex shapes and longer life-span. However, it remains a challenge to develop 3DP self-healing thermosets with sufficiently high strength and stiffness for structural applications. A thermally cured, DIW printing ink designed by Chandrasekaran *et al.*[16] resulted in a thermoset with triazine ring that exhibited high thermal stability and mechanical properties, with a T_g of 280 °C and tensile strength of 100 MPa. However, self-healing properties were not reported in their work. A polylactic acid blend reinforced by furan/maleimide networks has been reported by Davidson *et al.*[31] and Appuhamillage *et al.*[12] While prints with self-healing ability can be obtained via FFF method, the ultimate strength of such a material was in the range of 40-50 MPa, which does not meet the requirements of engineering grade plastics. Therefore, it remains necessary to develop structural grade 3DP thermosets that combine excellent mechanical properties with self-healing functionality. Herein, in this work, a 3DP ink composed of multi-furan/maleimide monomers and 10 wt.% ethylene glycol (EG) has been developed for the fabrication of mechanically strong and self-healing thermoset polymers. The synthetic route of the monomers, trifuran epoxy (TE) and 1,2-bis(2-maleimidoethoxy)ethane (BMIO), is shown in Fig. 1a. TE-BMIO-EG thermoset forms its entity after thermal curing of the ink at 80 °C, exhibiting a high tensile strength of 77 MPa and thermal reversibility at 120 ° C (Fig. 1b). Additionally, the low viscosity of the ink enables the fabrication of three-dimensional objects using a DIW approach. Samples printed in different orientations are shown to exhibit an isotropic behavior with regards to both tensile strength and fracture toughness. Moreover, up to three damage-healing cycles are achievable without significant deterioration in the healing efficiencies of the polymer. The measured healing efficiencies are found to be similar for both molded and printed samples. Finally, the reprocessing potential of the thermoset is demonstrated by a remolding test of the TE-BMIO-EG thermoset film.

Experimental

Materials

2,2'-(ethylenedioxy)bis(ethylamine), furfuryl alcohol, acetic acid, epichlorohydrin, furfurylamine, ethyl ether, and calcium hydride were purchased from Alfa Aesar. Maleic anhydride and tetrabutylammonium bromide (TBAB) were supplied by Acros Organics. Sodium sulfate (Na_2SO_4), sodium hydroxide (NaOH), hexanes, ethyl acetate (EtOAc), methylene chloride (DCM), methanol, and isopropanol were purchased from Fisher Scientific. Hydrogen peroxide was supplied by Sigma-Aldrich. Mold Star 30 silicone rubber was purchased for mold making from Smooth-On. Isopropanol was pre-dried over calcium hydride overnight, distilled under reduced pressure, and stored over dried molecular sieves (4Å). Other chemicals were used as received.

Synthesis

2-((oxiran-2-ylmethoxy)methyl)furan (1) A 1000-mL three-neck flask was equipped with a magnetic stirrer and charged with furfuryl alcohol (98 g, 1 mol) and TBAB (4.5 g). After the solvation of TBAB, epichlorohydrin (102 g, 1.1mol) was added dropwise within 1 hour under an inert atmosphere. The mixture was stirred for another 4 hours at room temperature. NaOH aqueous solution (160 mL, 50 wt.%) was then added to the mixture under vigorous stirring in an ice bath. The reaction mixture was stirred for 2 hours and then diluted with 200 mL water. The product was extracted with 50 mL ethyl ether three times and washed with 30 mL water three times. The solution was dried over Na_2SO_4 overnight and then evaporated to yield a red liquid as the crude product that was purified by chromatography (hexane). After evaporation of the solvent, 5 wt.‰ hydrogen peroxide was added to stabilize the epoxide against the development of color. The residue was kept under vacuum at 40 °C overnight to obtain the final product as a pale yellow liquid (Yield: 92.5 g, 60 %).

^{1}H NMR (400 MHz, $CDCl_3$): δ (ppm) 2.57 (dd, 1H), 2.75 (dd, 1H), 3.16 (dddd, 1H), 3.40 (dd, 1H), 3.72 (dd, 1H), 4.46 (d, 1H), 4.52 (d, 1H), 6.29-6.32 (m, 2H), 7.38 (s, 1H).

Trifuran epoxy (TE) Furfurylamine (9.7 g, 100 mmol), (1) (33.4 g, 210 mmol), and 150 mL isopropanol were added to a 500-mL two-neck flask. The reaction mixture was stirred and refluxed under a nitrogen atmosphere for 48 hours. The solution was concentrated under reduced pressure and taken up in 50 mL methanol. The resulting solution was washed with 30 mL hexanes three times and kept under vacuum at 110 °C overnight. The viscous oil was purified by chromatography (ethyl ether) to give an orange viscous oil (Yield: 38.5 g, 95 %).

^{1}H NMR (400 MHz, $CDCl_3$): δ (ppm) 2.51-2.64 (m, 2H), 3.16 (s, 2H), 3.35-3.51 (m, 4H), 3.70 (d, 2H), 3.80 (m, 2H), 4.45 (s, 4H), 6.14 (d, 1H), 6.25-6.31 (m, 5H), 7.32 (s, 1H), 7.36 (s, 2H).

1,2-bis(2-maleimidoethoxy)ethane (BMIO) A 1000-mL round flask was charged with maleic anhydride (95.3 g, 0.97 mol) and 400 mL acetic acid. After maleic anhydride was fully dissolved, 2,2'-(ethylenedioxy)bis(ethylamine) (40 g, 0.27 mol) was added dropwise within 20 minutes under vigorous stirring. The reaction mixture was refluxed overnight and concentrated under reduced pressure. The residue was taken up by 200 mL DCM and washed with 50 mL water. The water phase was then extracted with 20 mL DCM three times. The combined oil phase was washed with 40 mL water three times

and dried over Na_2SO_4 overnight. The resulting solution was concentrated and taken up with EtOAc to perform recrystallization induced by BMIO crystals, which can be obtained via chromatography (EtOAc/hexane 1:1). The recrystallized product was yellow powder (Yield: 30.0 g, 36 %).

^{1}H NMR (400 MHz, $CDCl_3$): δ (ppm) 3.53 (s, 4H), 3.58 (t, 4H), 3.68 (t, 4H), 6.68 (s, 4H).

Verification of DA reactions between monomers

Differential scanning calorimetry (DSC) was performed for TE and BMIO mixtures with a stoichiometric ratio on DSC Q2000 in a temperature window of 0 to 150 °C at a rate of 5 °C/min. ^{1}H Nuclear magnetic resonance (^{1}H NMR) spectra of monomers were obtained on a Varian MR400 spectrometer (400 MHz) at room temperature. DA and retro DA reactions between TE and BMIO were monitored and verified by ^{1}H NMR as well. TE (10 mg, 0.025 mmol) and BMIO (7.6 mg, 0.025 mmol) were dissolved in 600 µL DMSO-d_6 and loaded in an NMR tube. An NMR spectrum was recorded after the sample was heated overnight at 80 °C. The heat-treated sample was further heated at 120 °C for a duration of 30min, 1 hour, and 2 hours. The sample was then quenched in ice immediately after each thermal treatment, and the corresponding NMR spectrum was then collected under ambient conditions.

Rheological characterizations

The effect of ethylene glycol on the viscosity of the 3DP ink was investigated using a TA Instrument ARES rheometer equipped with a 20 mm diameter parallel plate geometry fixture. The shear viscosity of the samples at 120 °C was measured at shear rates ranging between 0.1 and 100 s^{-1}.

Preparation of the 3DP ink

Ethylene glycol (10 wt.%) was added to the TE and BMIO mixtures with a stoichiometric ratio. The mixture of ethylene glycol, TE, and BMIO was thoroughly mixed at 130 °C in a silicone-coated beaker. The mixture was degassed at 130 °C for 20 minutes before use.

DIW 3D printing

All printing objects were drawn by SOLIDWORK, and the corresponding G-codes were generated by Slic3r. The ink was loaded in a syringe barrel (Unity HiTemp, Nordson EFD) and printed on a modified 3D printer (AGS1500, Aerotech). Depending on the size of the printing objects, the syringe barrel was equipped with either an 18 or 22 gauge nozzle (Mcmaster Carr), and the printing parameters are shown in **Table 1**. The syringe barrel was equipped with a heater to reduce the ink viscosity. The ink was extruded through the nozzle using a pneumatic fluid dispenser (Ultimus V, Nordson EFD, 1-3 psi) onto a print bed coated with a thin layer of silicone rubber. All objects were printed at 120 °C and then cured at 80 °C overnight.

Table 1 Printing parameters of 18 and 22 gauge nozzles.

Parameters	18 gauge	22 gauge
Layer thickness (mm)	1.0	0.5
Infill density	40 %	60 %
Perimeter speed (mm/s)	13	15
Infill speed (mm/s)	13	15
Travel speed(mm/s)	70	70

Measurement of mechanical properties and self-healing performance

Tensile properties of the polymers were measured according to ASTM D1708, and the stress-strain data were collected with at least ten molded or printed dogbone shape samples. For the tensile tests, a preload of 2 N and a loading rate of 1 mm/min were used. Fracture toughness measurements were also conducted on at least ten molded or printed single-edge-notch bending (SENB) samples with dimensions shown in Fig. S8, using a preload of 0.8 N and a compression rate of 1 mm/min. All mechanical tests of the polymer were performed on an Instron 5982 load frame equipped with a 100 kN load cell at room temperature. Optical microscopy images of the fracture surface of SENB samples were obtained with a Nikon AZ100. SENB tests were also performed to measure the healing efficiency of TE-BMIO-EG thermoset. During each healing cycle, the damaged samples were placed in the mold and heat-treated at 120 °C for 2 hours. The samples were then cured at 80 °C overnight, followed by another SENB test to measure the new fracture load. Three damage-healing cycles were performed on each sample in order to obtain the healing efficiency for each cycle.

Remolding

An aluminum mold lined with a thin layer of silicone was made to cast a TE-BMIO-EG film (50 mm × 50 mm × 1 mm). The film was first cured at 80 °C overnight and then broken into pieces. The small pieces were placed between the mold and a silicone-coated aluminum plate, which were transferred to a hot press (Model 4836, Carver) with a load of 0.30 psi applied to the sample for 30 min at 120 °C. The resulting film was cooled down to room temperature and cured at 80 °C overnight for comparison.

Results and discussion

DA and Retro-DA Reaction between TE and BMIO

Since monomers bearing multi-furan/maleimide groups, TE and BMIO, have been successfully synthesized (Fig. S1-3), the reversible DA reaction between these two monomers needs to be examined in detail. Facilitated by the reversible formation of DA adducts between furan and maleimide, TE and BMIO cross-link in a specific temperature range and decouple at elevated temperatures. According to Chen *et al.*,[27] the DA reaction between furan and

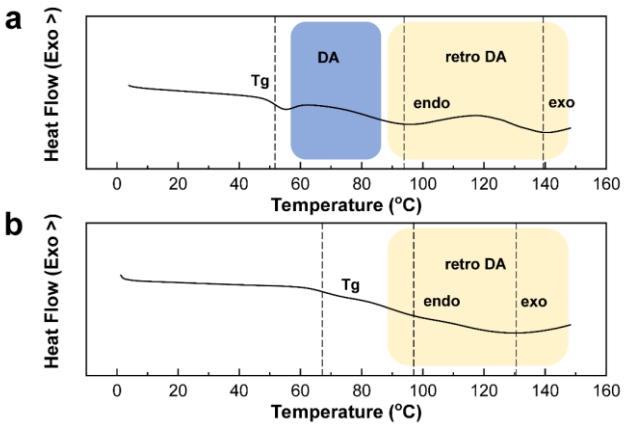

Fig. 2 DSC data of uncured and cured TE and BMIO mixtures. (a) The sample was prepared and quenched in ice immediately. (b) The sample was cured at 80 °C overnight.

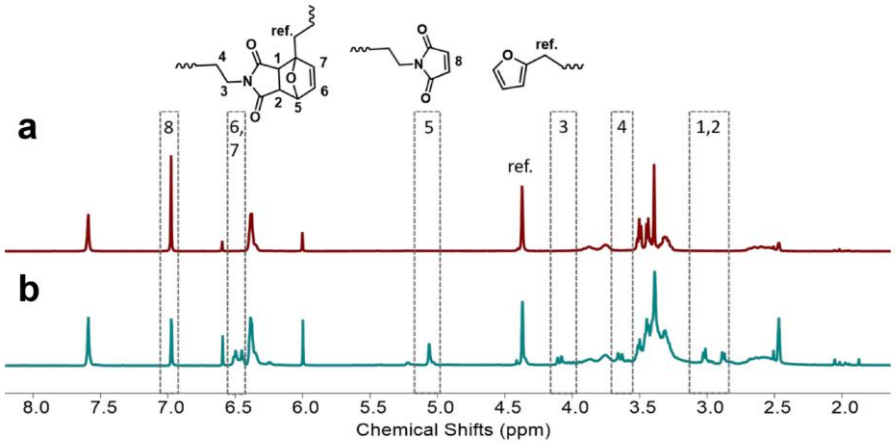

Fig. 3 ^{1}H NMR spectra of TE/BMIO blend in DMSO-d6. (a) The initial spectrum of unreacted TE/BMIO blend at room temperature. (b) The spectrum of the TE/BMIO blend at room temperature after heating at 80 °C overnight.

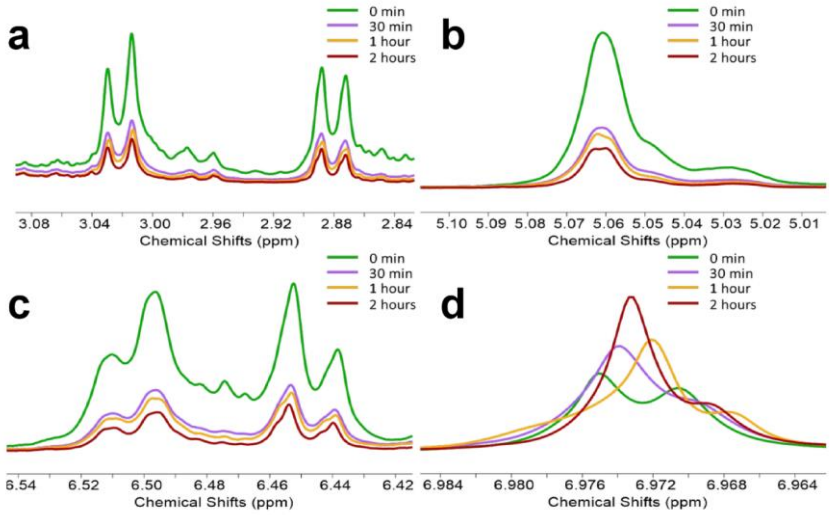

Fig. 4 ^{1}H NMR spectra of heat-treated TE/BMIO mixture at 120 °C over a period of 2 hours. Spectra are zoomed in in the range of (a) 2.84-3.08 ppm, (b) 5.01-5.10 ppm, (c) 6.42-6.54 ppm, and (d) 6.96-6.99 ppm to demonstrate the transition from DA adducts to TE/BMIO monomers.

maleimide is exothermic, while the retro DA reaction is endothermic. Therefore, TE and BMIO samples with different thermal histories are studied by DSC to determine the DA and retro DA temperature range. As shown in Fig. 2a, the uncured sample of TE and BMIO mixture shows a broad exothermic peak between 60 °C and 80 °C, indicating a DA reaction between TE and BMIO. However, unlike the formation of DA adducts with only a single exothermic peak observed, the uncoupling of DA adducts displays two endothermic peaks at 93 °C and 140 °C. According to Gandini *et al.*,[26] these two peaks indicate the cleaving of two DA-adducts: the *endo*-adduct and the *exo*-adduct, which are a pair of diastereoisomers. The cleaving temperature of the *endo*-adduct is lower than that of the *exo*-adduct due to its lower thermal stability.[32] Therefore, two DA-adducts have formed in the uncured sample during the ramp from 60 °C to 80 °C. Compared with the uncured sample, the DSC curve of the cured sample exhibits a higher glass transition temperature (T_g) at 68 °C and is devoid of any distinct exothermic peak between 60 and 80 °C (Fig. 2b), indicating the complete cross-linking between TE and BMIO monomers through DA reaction during the thermal curing. Similar to the uncured sample, the cured sample also exhibits two endothermic peaks at 97 °C and 131 °C, which indicates the formation of the *endo*-adduct and the *exo*-adduct during the curing process. However, the cured sample has a greater extent of *exo*-adduct than that of the uncured sample as it shows a more prominent endothermic peak of *exo*-adduct in Fig. 2b, implying better thermal stability than that of the uncured sample. Based on the thermal analysis above, 80 °C and 120 °C are selected as the curing and healing temperatures of the material, respectively, as they generally fall in the range of DA and retro DA reaction temperature.

Since DSC data cannot provide direct proof of the (retro) DA reactions between TE and BMIO, ^{1}H NMR is performed to monitor the structural change of TE/BMIO monomers and the resulting DA adducts overtime during the (retro) DA reactions. TE/BMIO monomer blends with a molar ratio of 1:1 are prepared to avoid the formation of the insoluble thermoset during the heating process. The ^{1}H NMR spectra of the original sample and the thermally treated sample are shown in Fig. 3a and Fig. 3b, respectively, where new peaks of the thermally treated sample indicate the occurrence of DA cycloaddition. These new peaks correspond to the 2 H's from the DA adduct at 2.88 and 3.02 ppm, 4 H's from -CH_2CH_2N- on reacted BMIO

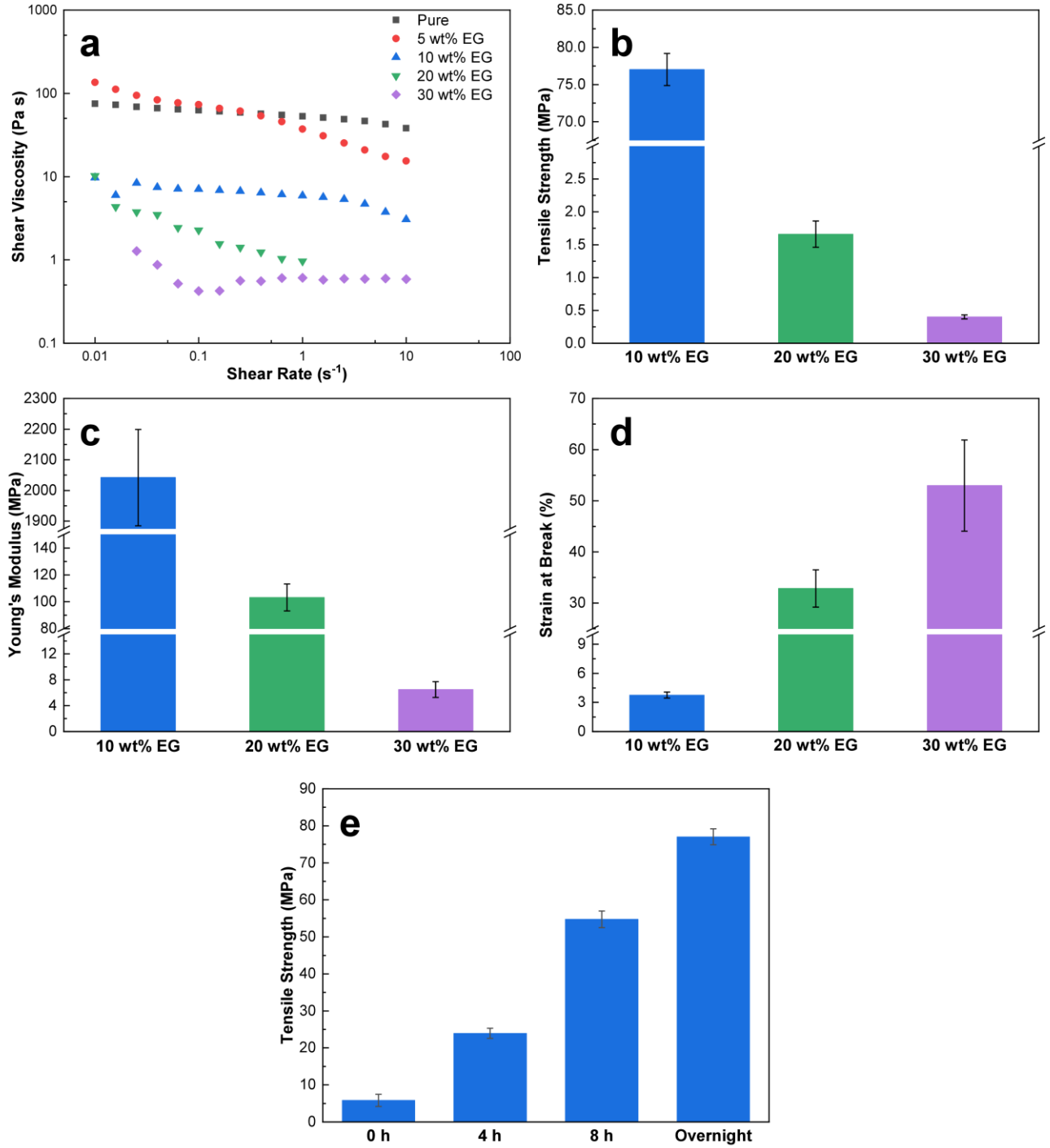

Fig. 5 (a) The shear viscosity at 120 °C of the TE-BMIO blend diluted with 0, 5, 10, 20, and 30 wt.% EG. (b) The tensile strength, (c) Young's modulus, and (d) strain at break of the cured TE-BMIO blend diluted with 10, 20, and 30 wt.% EG. (e) The tensile strength of the TE-BMIO blend diluted with 10wt.% EG after curing at 80 °C for 0 h, 4 h, 8 h, and overnight (> 12 h).

at 3.65 and 4.10 ppm, 1 H from reacted furan at 5.06 ppm, and 2 H's from the newly formed double bond on furan at 6.45 and 6.50 ppm. Another observation is the decrease in the BMIO double bond peak intensity at 6.98 ppm with respect to the reference peak at 4.38 ppm, implying the consumption of maleimide during the DA reaction of TE and BMIO. To further verify the retro DA reaction of the DA adducts, the sample heated at 80 °C in the previous step are then monitored at 120 °C. As shown in Fig. 4a, b, and c, peaks from DA adducts experience a decrease in intensity, signaling a decrease in the concentration of DA adducts at 120 °C as a function of time. Meanwhile, a growth in maleimide peak intensity is observed at 6.97 ppm with increasing time (Fig. 4d), as the BMIO component is being recovered during the retro DA reaction. The entire ^{1}H NMR spectra discussed above are shown in Fig. S4 and S5 with detailed peak assignments.

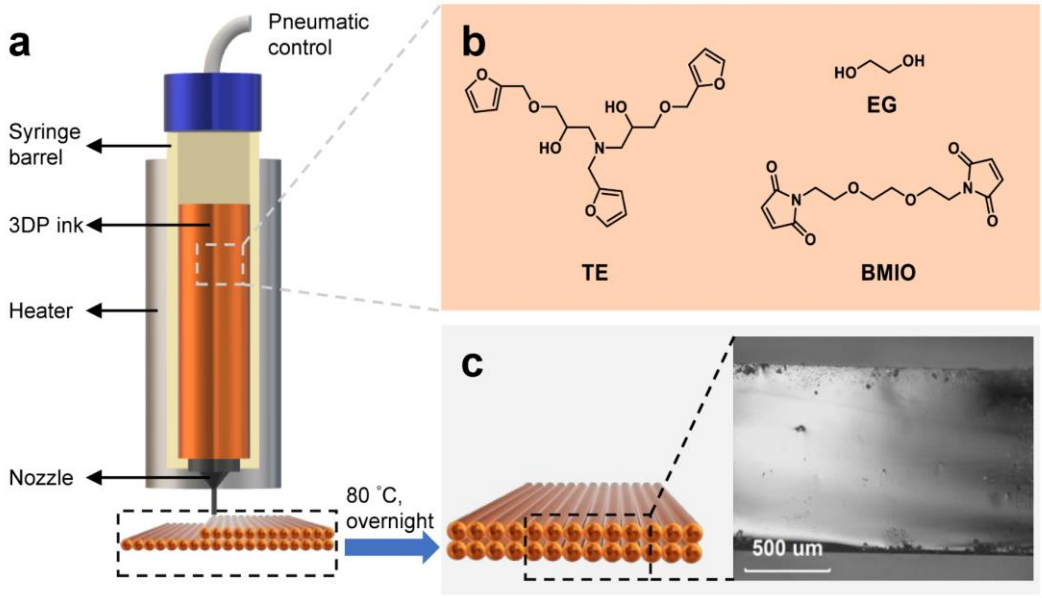

Fig. 6 Schematic of the 3DP process of the TE-BMIO-EG ink. (a) 3DP printer setup modified by a heater with temperature control. (b) Compositions of the 3DP ink and the chemical structures of the components. (c) Optical microscopy image of the cross-section of the printed material.

Fig. 7 (a) The original design of a 7 mm × 7 mm × 7 mm cube. (b) The image of the as-printed cube. (c) The printed cube after curing overnight.

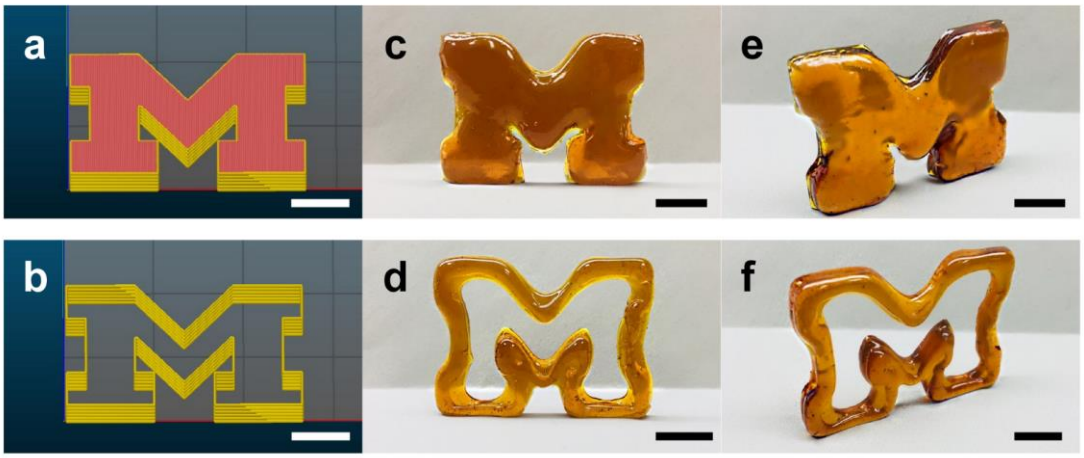

Fig. 8 Images of the designed and printed objects. (a) and (b) are the initial design of the 3DP objects. (c), (d), (e), and (f) are the photos of the corresponding prints from different views. Scale bars in a-f: 1cm.

Optimization of 3DP ink compositions and curing time

The compositions of 3DP ink containing TE and BMIO are further explored via the addition of diluents to achieve the best processability of the ink. Monomers bearing multi-furan/maleimide groups, TE and BMIO, are stoichiometrically used in the initial 3DP ink. However, the poor processability of the monomer blend derived from its high viscosity results in an extremely difficult degassing process and prompts the formation of voids in the cured polymer. Therefore, ethylene glycol (EG) is added into the mixture as the diluent to improve the processability of the 3DP ink, as EG does not react with TE or BMIO. Moreover, the high boiling point (198 °C) of

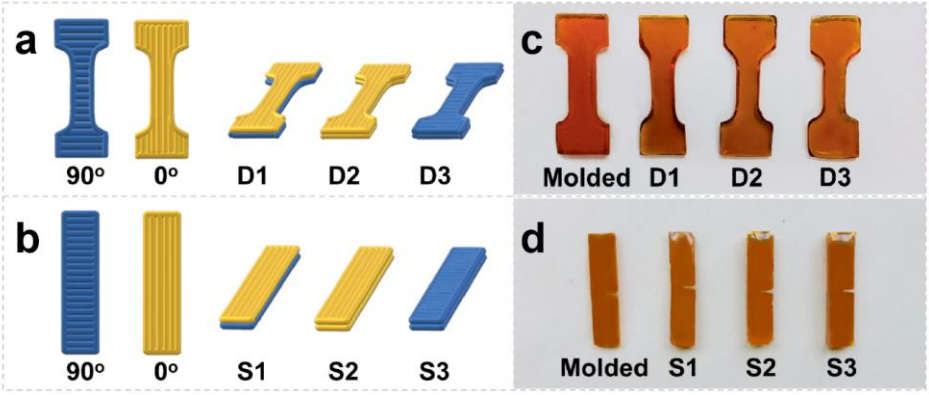

Fig. 9 (a), (b) Illustrations of the printing orientation and infill patterns of each layer. D1, D2, and D3 are dog-bone shape samples printed in different directions and layer features. S1, S2, and S3 are SENB samples printed without pre-cracks. (c) Molded and printed D1, D2, D3 dogbone shape samples. (d) Molded and printed S1, S2, S3 pre-cracked SENB samples.

EG ensures its stability during printing. As shown in Fig. 5a, a significant reduction in viscosity of the monomer blend is observed in blends containing 10, 20, and 30 wt.% EG. The tensile strength of the molded samples containing 10, 20, and 30 wt.% EG is also measured to study the influence of EG upon the mechanical properties. Neat samples are not tested due to the porosity in samples caused by high viscosity. As can be seen in Fig. 5b and c, the tensile strength and modulus of specimens have decreased dramatically with increasing concentration of EG in the monomer blend, which implies that the addition of excessive diluent degrades the mechanical properties of the cured ink. Moreover, the cured material tends to be more malleable with a higher percentage of EG added, as indicated by the increasing strain at break shown in Fig. 5d. To simultaneously satisfy processability requirements and maximize mechanical performance, the TE-BMIO monomer blend diluted with 10 wt.% EG is selected as 3DP ink and further studied in the following sections. Additionally, it is also necessary to discuss the curing time of the ink in order to efficiently achieve the ideal mechanical performance, because the DA reaction takes a considerably long time (> 3 h) to complete in polymeric systems.[33] Therefore, the tensile strength of the molded 3DP ink samples cured for 0, 4, 8 h, and overnight (> 12 h) has been measured with the result shown in Fig. 5e. Compared with other groups, samples cured overnight shows a higher tensile strength (77.02 ± 2.15 MPa), which demonstrates the necessity of extended curing time (> 12 h).

3DP of the TE-BMIO-EG Ink

In order to realize the optimal printing condition, DIW equipment is designed specifically for TE-BMIO-EG ink, with the setup shown in Fig. 6a. The printing process is enabled by a pneumatic system where the continuous and constant air pressure allows the stable extrusion of the ink. At printing temperature (120 °C), the low viscosity ink is deposited onto a substrate kept at room temperature, and the ink is thus solidifying and holding its shape upon cooling. The deposited material is then cured at 80 °C overnight to obtain the TE-BMIO-EG thermoset. Considering the possible shape changes caused by the thermal treatment, we printed a 7 mm × 7 mm × 7 mm cube and measured its dimensions before and after cure (Fig. 7) to investigate the influence of thermal curing upon the shape of the prints. The actual dimensions of the as-printed cube are 7.03 mm × 7.05 mm × 6.85 mm, whereas those of the cured one are 6.93 mm × 6.90 mm × 6.76 mm, showing a 5 % shrinkage after cure due to the higher cross-link density in the resin. Overall, the curing process causes a small portion of shrinkage, yet the shape change of the prints is not discernable, as shown in Fig. 7b and c. Another major challenge of thermosets produced by 3DP is the ability to deposit the ink without the formation of rough surfaces and void space between printed filaments. Prints with such undesirable features usually suffer from severely degraded mechanical properties.[28] However, as shown in Fig. 6c, the developed ink in this work results in no inter-filament voids in the cured prints. Due to the low viscosity of the 3DP ink, the printed ink merges with adjacent solidified filament upon cooling and fills any formed voids. Nevertheless, the low viscosity of the ink also leads to a low printing resolution. Compared to the original design of the 3DP objects (Fig. 8a, b), the final prints shown in Fig. 8c, d, e, and f lack some geometric details such as sharp edges and angles due to the slow cooling of the printed ink.

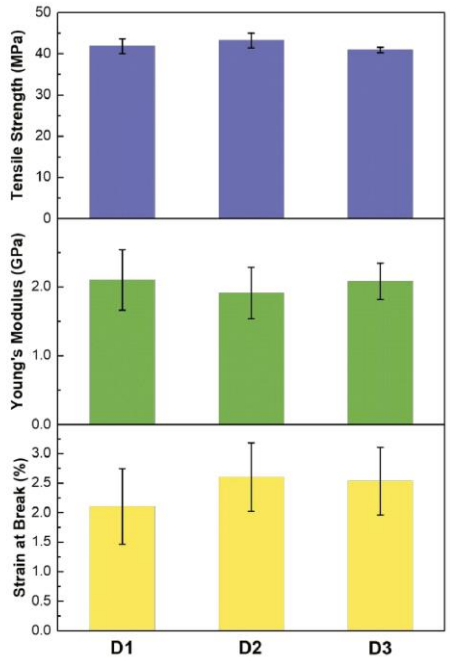

Fig. 10 The tensile strength, Young's modulus, and strain at break of the printed samples D1, D2, and D3.

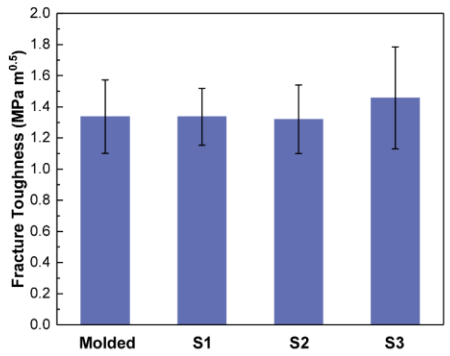

Fig. 11 Fracture toughness of molded SENB samples and printed SENB samples S1, S2, and S3.

Mechanical Properties of the Printed Polymer

As discussed in the previous section, the prints display no inter-filaments voids, thus potentially granting the thermoset prints isotropic mechanical properties due to the uniformity of their internal structure. To investigate this, we perform tensile and SENB tests on samples printed in different orientations. Two printing patterns are adopted for the printing of each layer. The printing pathway parallel with the long axis is defined as 0° printed, whereas the pathway perpendicular to the long axis is defined as 90° printed. Printing of dogbone shape samples D1 and SENB sample S1 follows an alternating 0°/90° layer configuration, whereas D2 and S2 are 0° printed, D3 and S3 are 90° printed, as shown in Fig. 9a and 9b. The tensile properties of the samples printed in the D1, D2, and D3 configuration is shown in Fig. 10. The tensile strengths of D1, D2, and D3 are measured to be 40.87 ± 1.03, 44.73 ± 1.16, and 40.91 ± 0.63 MPa, respectively. One-way ANOVA analysis (α = 0.05) of the obtained tensile strength data sets confirms that the printing orientation is not a significant factor for the mechanical properties of the printed thermosets. However, relative to the molded samples (77.02 ± 2.15 MPa), the printed samples suffered from a maximum decrease of 47% in tensile strength. This is believed to be caused by voids created by air bubbles in the printed samples, which can be observed on cross-sections of the D2 samples using optical imaging (Fig. S6 and S7). The diameters of bubbles found in the printed samples range from 50 to 200 µm, which can considerably weaken the mechanical properties of the prints. Those air bubbles could be caused by (1) trapped air between the fused filaments; and (2) the direct contact between ink and airflow. After looking into the locations of the bubbles on the cross-sectional slices, we believe that the latter to be the main cause, because most bubbles are not found near the boundaries between the printed filaments (Fig. S7). Although the tensile strength of the printed dogbone samples is not comparable to that of the molded samples, the decrease in mechanical properties is still improved comparing with previous studies. According to a study on 3DP of Acrylonitrile-butadiene-styrene (ABS) by Ahn et al., the reduction in tensile strength can be as much as 90 % comparing to molded samples.[34]

To exclude the influence of voids caused by air bubbles, printed SENB samples without visible voids around the pre-crack are selected for fracture toughness measurement and are compared with molded samples. The results of SENB tests for both molded and printed samples are shown in Fig. 11. The fracture toughness of molded samples, S1, S2, and S3 are 1.34 ± 0.24, 1.34 ± 0.18, 1.32 ± 0.22, and 1.46 ± 0.33 MPa $m^{0.5}$, respectively. Evaluated by one-way ANOVA tests (α = 0.05), the printing direction is found to have no effect on the fracture toughness of the printed samples. Moreover, fracture toughness of printed and molded samples are almost identical, thus indicating the infill pattern itself does not have a negative influence upon the material's mechanical properties despite the effects of bubble-induced voids.

Self-healing Performance and Repocessability

As has been verified in previous sections, the 3DP ink developed in this work contains furan and maleimide groups, which experience DA reaction to form DA adducts around 80 °C and retro DA reaction to decouple around 120 °C. This feature enables self-healing of the material at damaged sites, where DA adducts cleave to produce free segments with furan and maleimide at 120 °C, and form again to heal the cracks at 80 °C as the free furan and maleimide segments fill the defects and recouple. To determine the self-healing capacity of the developed TE-BMIO-EG thermoset, three cycles of damage-healing experiments are carried out for both molded and printed SENB samples. Since the internal structure of the prints has been proven to be isotropic, the healing performance of the prints should be consistent regardless of printing orientations. Hence, SENB tests are conducted with specimens printed in different printing orientations (Fig. 9b) to confirm the hypothesis. The healing efficiencies are calculated using Equation (1) based on the maximum load obtained during each SENB test as below:

$$\textit{Healing efficiency}\ (\%) = \frac{\textit{The max load of the healed sample}\ (N)}{\textit{The max load of the original sample}\ (N)} \times 100\% \quad (1)$$

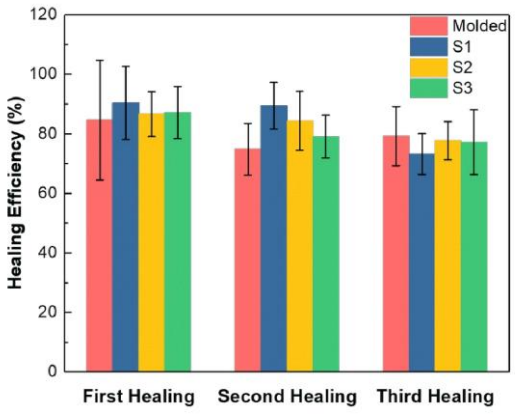

Fig. 12 Healing efficiencies of molded samples and printed samples S1, S2, and S3 for the first three damage-healing cycles.

Table 2 Self-healing efficiencies of samples printed in different directions and the resulting *p*-value of each healing

Samples	1st Healing (%)	2nd Healing (%)	3rd Healing (%)
S1	90.44 ± 12.30	89.48 ± 7.76	73.22 ± 6.85
S2	86.66 ± 7.53	84.42 ± 9.84	77.69 ± 6.40
S3	87.13 ± 8.79	79.07 ± 7.17	77.24 ± 10.93
p-value	0.87	0.29	0.76

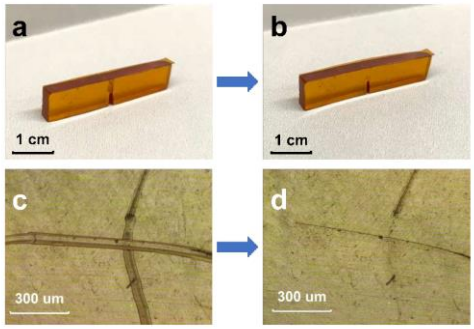

Fig. 13 (a) A cracked TE-BMIO-EG SENB sample. (b) The cracked sample after healing. (c) Scratches on the thermoset surface. (d) The healed scratches after the heat treatment.

Fig. 14 The initial TE-BMIO-EG thermoset film, the broken film, and the remolded film. The logo beneath the film demonstrates the transparency of the film.

The results of both printed and molded samples are shown in Fig. 12, and the detailed values are listed in Table S1. The representative fracture behavior of molded and printed samples during each damage-healing test is also shown in Fig. S9. The highest healing efficiencies (~85%) are observed during the first healing cycle for both molded and printed samples. Although the healing efficiency undergoes a slight decrease with increasing damage cycles, the strength recovery is still as high as 75 % after three damage-healing tests, demonstrating a sustainable healing capacity of the material. One-way ANOVA tests ($\alpha = 0.05$) are performed with S1, S2, and S3 for each healing cycle to study the effects of infill patterns on healing efficiency. The *p*-values obtained for the first, second, and third healing shown in Table 2 suggest no changes in the self-healing capacity of the polymer as a result of different printing infills. The healing ability of the material is demonstrated in Fig. 13, as the crack within the molded sample (Fig. 13a) is clearly observed to heal (Fig. 13b) after heating at 120 °C for 2 hours. The healing of the damaged sites is observed not only in the material but also on the material surface. Optical images provide microscopic insights into the healing of surface defects, as shown in Fig. 13c, d. The scratches on the surface of TE-BMIO-EG thermoset created by a needle vanish after the same heat treatment is applied.

As has been verified in this section, the reversible DA reaction enabled a 75% or higher recovery in mechanical properties of TE-BMIO-EG thermoset, even after multiple healing cycles. Therefore, it is possible that the material can be reprocessed. Hence, a remolding experiment is performed to explore the processability potential of the polymer (Fig. 14). Pressure and heat are applied to the small pieces of the original film, molding the broken material into a transparent film without discernable differences in color compared to the initial film. The results of the remolding test open up possibilities in the reprocessing ability and the recycling aspect of the thermoset, which would save more resources and energy and offer a more eco-friendly option than other traditional thermosets.

Conclusions

In brief, a novel 3DP ink is developed for the fabrication of a self-healing thermoset. The material exploits the Diels-Alder reaction between furans and maleimides, and the molded samples achieve a tensile strength (77 MPa) comparable to that of engineering-grade plastics. The thermal reversibility of furan-maleimide cross-links enables high strength recovery of up to 85% at elevated temperatures. Printing orientations are also found to be insignificant to either the mechanical properties or the healing performance of the polymer due to the isotropic internal structure of the prints. This isotropic characteristic is derived from the absence of gaps between printed filaments caused by the low viscosity of the 3DP ink. The reversible Diels-Alder reaction also enables the reprocessing of the material, providing new possibilities for the recycling of 3DP thermosets. The high strength, self-healing functionality, and reprocessing ability of the material create opportunities for the development of 3DP thermosets with exceptional mechanical properties, long service life, and recycling potentials.

Acknowledgements

The authors sincerely thank Dr. Ryan Hall from Larson group for the technical support for rheology testing. The authors would also like to thank the Air Force Office of Scientific Research for their financial support under contract number FA9550-16-1-0087.

References

1 A. Reiser, M. Lindén, P. Rohner, A. Marchand, H. Galinski, A. S. Sologubenko, J. M. Wheeler, R. Zenobi, D. Poulikakos, and R. Spolenak, *Nat. Commun.*, 2019, **10**, 1-8.
2 J. Dong, C. Mei, J. Han, S. Lee, and Q. Wu, *Addit. Manuf.*, 2019, **28**, 621-628.
3 S. Deng, J. Wu, M. D. Dickey, Q. Zhao, and T. Xie, *Adv. Mater.*, 2019, **31**, 1-7.
4 D. Lei, Y. Yang, Z. Liu, S. Chen, B. Song, A. Shen, B. Yang, S. Li, Z. Yuan, Q. Qi, and L. Sun, *Mater. Horiz.*, 2019, **6**, 394-404.
5 M. Zarek, M. Layani, I. Cooperstein, E. Sachyani, and D. Cohn, *Adv. Mater.*, 2016, **28**, 449-4454
6 L. Ouyang, C. B. Highley, C. B. Rodell, W. Sun, and J. A. Burdick, *ACS Biomater. Sci. Eng.*, 2016, **2**, 1743-1751
7 S. K. Moon, Y. E. Tan, J. Hwang, and Y. Yoon, *Int. J. Precis. Eng. Manuf.*, 2014, **1**, 223-228.
8 T. Raju, Y. Ding, Y. He, L. Yang, P. Moldenaers, W. Yang, T. Czigany, and S. Thomas, *Polymer*, 2008, **49**, 278-294.
9 R. J. Iredale, C. Ward, and I. Hamerton, *Prog. Polym. Sci.*, 2017, **69**, 1-21.
10 V. Schimpf, A. Asmacher, A. Fuchs, and B. Bruchmann, *Macromolecules*, 2019, **52**, 3288-3297.
11 S. C. Ligon-auer, M. Schwentenwein, C. Gorsche, and R. Liska, *Polym. Chem.*, 2016, **7**, 257-286.
12 G. A. Appuhamillage, J.C. Reagan, S. Khorsandi, J. R. Davidson, W. Voit, and R. A. Smaldone, *Polym. Chem.*, 2017, **8**, 2087-2092.

13 C. Mcilroy and P. D. Olmsted, *Polymer*, 2017, **123**, 376-391.
14 K. Yang, J. C. Grant, P. Lamey, A. Joshi-Imre, B. R. Lund, R. A. Smaldone, and W. Voit, *Adv. Funct. Mater.*, 2017, **27**, 1700318.
15 Q. Shi, K. Yu, X. Kuang, X. Mu, C. K. Dunn, M. L. Dunn, T. Wang, and H. J. Qi, *Mater. Horiz.*, 2017, **4**, 598-607.
16 C. B. Highley, C. B. Rodell, and A. Jason, *Adv. Mater.*, 2015, **27**, 5075-5079.
17 S. Chandrasekaran, E. B. Duoss, M. A. Worsley, and J. P. Lewicki, *J. Mater. Chem. A*, 2018, **6**, 853-858.
18 X. Kuang, K. Chen, C.K. Dunn, J. Wu, V. C. Li, and H.J. Qi, *ACS Appl. Mater. Interfaces*, 2018, **10**, 7381-7388.
19 D.R. Berry, B.K. Díaz, A. Durand-Silva, and R. A. Smaldone, *Polym. Chem.*, 2019, **10**, 5979-5984.
20 Z. Miao, J. Seo, and M. A. Hickner, *Polymer*, 2018, **152**, 18-24.
21 P. Sanders, A. J. Young, Y. Qin, K. S. Fancey, M. R. Reithofer, R. Guillet-Nicolas, F. Kleitz, N. Pamme, and J. M. Chin, *Sci. Rep.*, 2019, **9**, 388.
22 S. A. Mcdonald, S. B. Coban, N. R. Sottos, and P. J. Withers, *Sci. Rep.*, 2019, **9**, 17773.
23 I. P. S. Qamar, N. R. Sottos, and R. S. Trask, *Multifunctional Materials*, 2020, **3**, 013001.
24 D. Yu, M. Zhi, and M. Qiu, *Prog. Polym. Sci.*, 2015, **49**, 175-220.
25 S. R. White, B. J. Blaiszik, S. L. Kramer, S. C. Olugebefola, J. S. Moore, and N. R. Sottos, *Am. Sci.*, 2011, **99**, 392-399.
26 A. Gandini, *Prog. Polym. Sci.*, 2013, **38**, 1-29.
27 X. Chen, M. A. Dam, K. Ono, and A. Mal, *Science*,2002, **295**, 1698-1703.
28 Y. Heo, and H. A. Sodano, *Adv. Funct. Mater.*, 2014, **24**, 5261-5268
29 L. Feng, Z. Yu, Y. Bian, J. Lu, and X. Shi, *Polymer*, 2017, **124**, 48-59.
30 A. A. Kavitha and N. K. Singha, *ACS Appl. Mater. Interfaces*, 2009, **1**, 1427-1436.
31 J. R. Davidson, G. A. Appuhamillage, C. M. Thompson, W. Voit, and R. A. Smaldone, *ACS Appl. Mater. Interfaces*, 2016, **8**, 16961-16966.
32 K. Roos, E. Dolci, S. Carlotti, and S. Caillol, *Polym. Chem.*, 2016, **7**, 1612-1622.
33 A. Cuvellier, R. Verhelle, J. Brancart, B. Vanderborght, G. Van Assche, and H. Rahier, *Polym. Chem.*, 2019, **10**, 473-485.
34 S. H. Ahn, M. Montero, D. Odell, S. Roundy, and P. K. Wright, *Rapid Prototyp. J.*, 2002

Table of Contents Entry:

3D Printing of Self-Healing, High Strength, and Reprocessable Thermoset

Tianyu Yuan, [a] Lisha Zhang, [a] Tony Li, [b] Ruowen Tu, [b] Henry A. Sodano*[a,b,c]

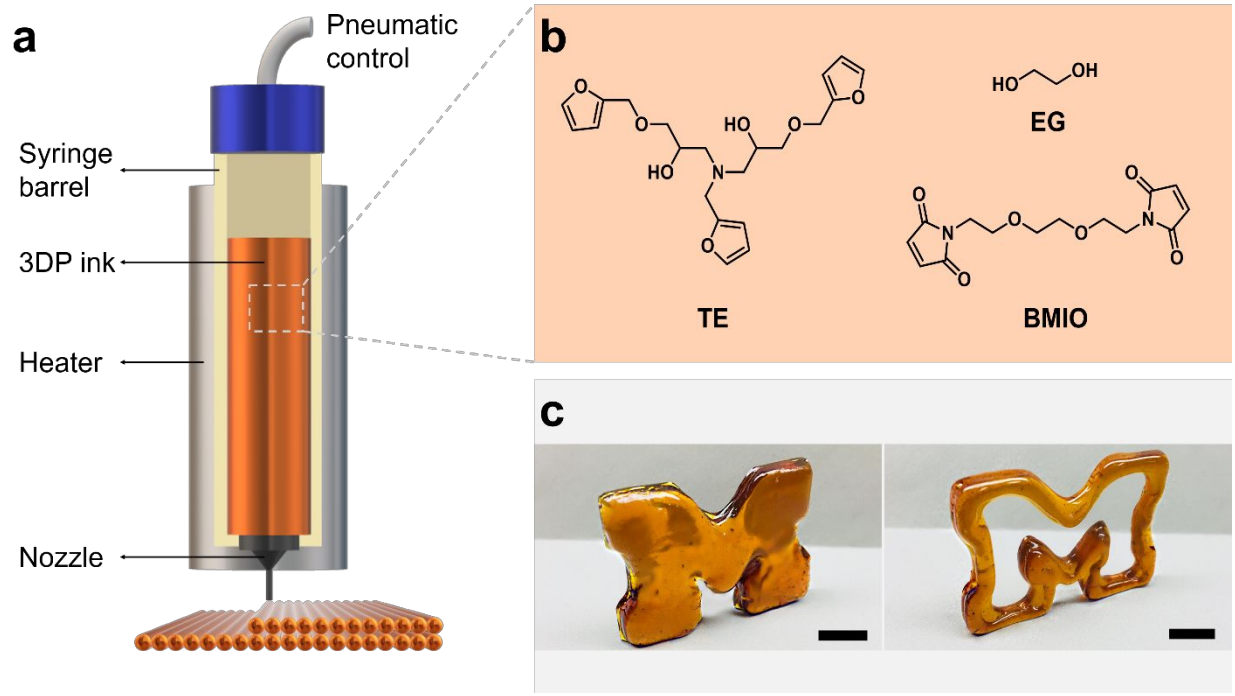

A furan-maleimide based 3D printing ink for the fabrication of a self-healing and high strength thermoset with recycling potentials.